EUROPEAN SYNCHROTRON RADIATION FACILITY

INSTALLATION EUROPEENNE DE RAYONNEMENT SYNCHROTRON

ESRF

Experiment Report Form

The double page inside this form is to be filled in by all users or groups of users who have had access to beam time for measurements at the ESRF.

Once completed, the report should be submitted electronically to the User Office using the **Electronic Report Submission Application:**

http://193.49.43.2:8080/smis/servlet/UserUtils?start

Reports supporting requests for additional beam time

Reports can now be submitted independently of new proposals – it is necessary simply to indicate the number of the report(s) supporting a new proposal on the proposal form.

The Review Committees reserve the right to reject new proposals from groups who have not reported on the use of beam time allocated previously.

Reports on experiments relating to long term projects

Proposers awarded beam time for a long term project are required to submit an interim report at the end of each year, irrespective of the number of shifts of beam time they have used.

Published papers

All users must give proper credit to ESRF staff members and proper mention to ESRF facilities which were essential for the results described in any ensuing publication. Further, they are obliged to send to the Joint ESRF/ ILL library the complete reference and the abstract of all papers appearing in print, and resulting from the use of the ESRF.

Should you wish to make more general comments on the experiment, please note them on the User Evaluation Form, and send both the Report and the Evaluation Form to the User Office.

Deadlines for submission of Experimental Reports

- 1st March for experiments carried out up until June of the previous year;
- 1st September for experiments carried out up until January of the same year.

Instructions for preparing your Report

- fill in a separate form for each project or series of measurements.
- type your report, in English.
- include the reference number of the proposal to which the report refers.
- make sure that the text, tables and figures fit into the space available.
- if your work is published or is in press, you may prefer to paste in the abstract, and add full reference details. If the abstract is in a language other than English, please include an English translation.

ESRF	**Experiment title:** **In situ monitoring of fast nucleation, growth and superlattice formation of gold nanoparticles by time-resolved small angle x-ray scattering**	**Experiment number**: SC1923
Beamline: ID02	**Date of experiment**: from: 03th march 2006 to: 06th march 2006	**Date of report**: 30th august 2007
Shifts: 9	**Local contact(s)**: Stéphanie Finet	*Received at ESRF:*

Names and affiliations of applicants (* indicates experimentalists):

Benjamin Abécassis

Fabienne Testard

Olivier Spalla

Philippe Barboux

Report:

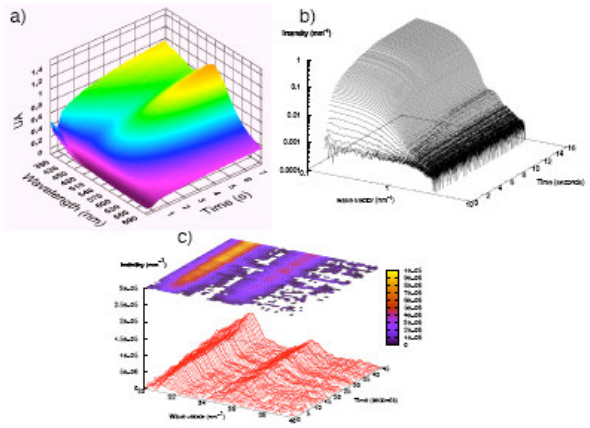

Figure 1: formation of AuNP by in situ UV-visible, SAXS and WAXS with the decanoic acid ligand: a) UV-vis spectra as a function of time. The decrease of the 400 nm peak in the first instants shows the disparition of Au(III) before the appearance of the plasmon band at ca 540 nm. b) SAXS patterns as a function of time. Just after the mixing and until t=140 ms, the signal is very weak in the whole scattering range indicating a very low structuration of the solution and the absence of nanoparticles. During the first second, a large increase of the intensity at small q is visible, with a cross-over to a rapidly decreasing intensity at large q. As the time of reaction increases beyond one second, the intensity at low q still devellops meanwhile the cross-over of regime at large q is reached for a lower q value. In this large q regime, an oscillation is even measurable around 3 nm^{-1} which is characteristic of the form factor of nanometric objects. This oscillation shifts with time toward lower q indicating that the scattering objects are growing in size. c) WAXS patterns as a function of time. The two peaks (110) and (200) are clearly visible and their intensity increases with time.

We have probed *in situ* by SAXS/WAXS the nucleation and growth of gold nanoparticles. The use of a fast mixing stopped flow device enables the assesment of the whole particle formation process with a 200 ms time resolution. The number of particles, their size distribution and the yield of the reaction is determined in real time through the

quantitative analysis of the SAXS datas at the absolute scale. Two ligands exhibit drasticly different behaviors. When an alkanoic acid is used a nucleation phase of 1 s is followed by a growth step whose rate is limited by the reaction of the monomers at the interface. At the opposite, when an alkylamine is used, the nucleation rate is increased by a an order of magnitude, thus annealing growth by lack of monomer and yielding R = 1 nm particles in 2 second as compared to R = 3.7 nm in 12 s in the acid case.

In the last few years, the control over the size, shape and composition of inorganic nano-crystals has became far more complete than ever expected[1–3] and now the reaction conditions can be tuned to yield a specific product. However, the predictive character of these essentially empirical approaches remain incomplete and precisely designed experiments are now mandatory to reveal the mechanisms at work in the formation of nanoparticles.[4] During the formation of nanoparticles (NP), the time and length scales of the nucleation and growth processes and their inherent transient nature have hindered the possibility of direct real-time measurements.

Gold nanoparticles (AuNP) are among the oldest and most studied nanoscale materials[7] due to their important potential applications in biotechnology[8] and catalysis.[9] In this paper, we investigate the monophasic synthesis described by Jana *et al.*[10] The AuNP are obtained through the reduction by a borohydride salt (BH_4^-) of a gold salt solubilised in toluene by a cationic surfactant (DDAB) in the presence of an excess of alkyl derivative ligands, either decylamine or decanoic acid (see supporting information). Fast and reproducible mixing of the two precursor solutions (gold salt and reducing agent/ligand solutions) was ensured by the use of a stopped flow device.[11–13] The AuNP form in a few seconds and the experimental set-up enables the monitoring of their formation since the very beginning of the reaction (dead time of 16 ms) with a time resolution ranging from 3 ms in the case of the UV-visible experiments to 130 ms for the small angle X-ray scattering (SAXS) and 800 ms for the wide angle X-ray scattering (WAXS), performed at the ID02 beamline. Figure 1 presents the temporal evolution of the different physical quantities. SAXS is very efficient to assess unambiguously the number and size distribution of the nuclei and particles during the reaction. Indeed, a solution of atomic gold solely scatters a flat and very weak signal and after a correct treatment the scattering signal only comes from the contrast between the growing AuNP and the solvent. In that case, the volume fraction Φ of the AuNP can be measured with time using a general property of scattering diagrams (Eq 1):

$$\int I(q)q^2 \mathrm{dq} = 2\pi^2 (\Delta\rho)^2 \Phi(1-\Phi) \tag{1}$$

where $\Delta\rho$ is the scattering length density contrast between gold and toluene ($\Delta\rho^2 = 1.519\,10^{20}$ mm^{-4}). The left term is calculated from experimental scattering diagram and the right term allows to extract the volume fraction of AuNp in the solution. For a total conversion of atomic gold to nanoparticles, the maximal value of Φ would be $\Phi_{max} = C_0 \times V_m$ where C_0 is the initial concentration of Au(III) and V_m the molecular volume of Au(0) in bulk gold. Thus, the yield of the reaction is obtained at any time t by : $Y = \frac{\Phi}{\Phi_{max}}$ as shown in figure 2. Two conclusions can be drawn: for the acid case the reaction lasts 12 s and 53 % of gold atoms are transferred in the particles at the end. For the amine case, the final yield is the same but the plateau is reached in 3 seconds confirming the fact that the reaction is much faster.

In order to extract the number density n, the radius r_0 and the polydispersity σ of the nuclei and growing nanoparticles, the calculated scattering from a population of objects is compared to the SAXS data and the distribution adjusted to optimize the fitting using a Levenberg-Marquardt algorithm. The best results were obtained with the total scattered intensity per unit volume (Eq 2) calculated for a population of spheres with a gaussian distribution :

$$I(q) = \frac{1}{V}\frac{d\Sigma}{d\Omega} = \Delta\rho^2 (n \int f(r) V(r)^2 P(q,r)\, \mathrm{d}r) \tag{2}$$

where $P(q,r) = \frac{9(\sin(qr) - qr\cos(qr))^2}{(qr)^6}$ is the form factor of a sphere. The influences of n, r_0 and σ are strongly decoupled, providing unambiguous results for the fitting process. The radius centre r_0 and σ act on the transition regime of the SAXS pattern where the intensity starts to decrease and on the attenuation of the form factor oscillations at high q whereas n only acts on the total amplitude. The agreement of the calculated intensities with the experimental diagrams is almost perfect as shown in figure 3 (see also supporting information) yielding for every time the size distribution of particles 3 c) and providing a solid ground to discuss the time evolution of the different parameters.

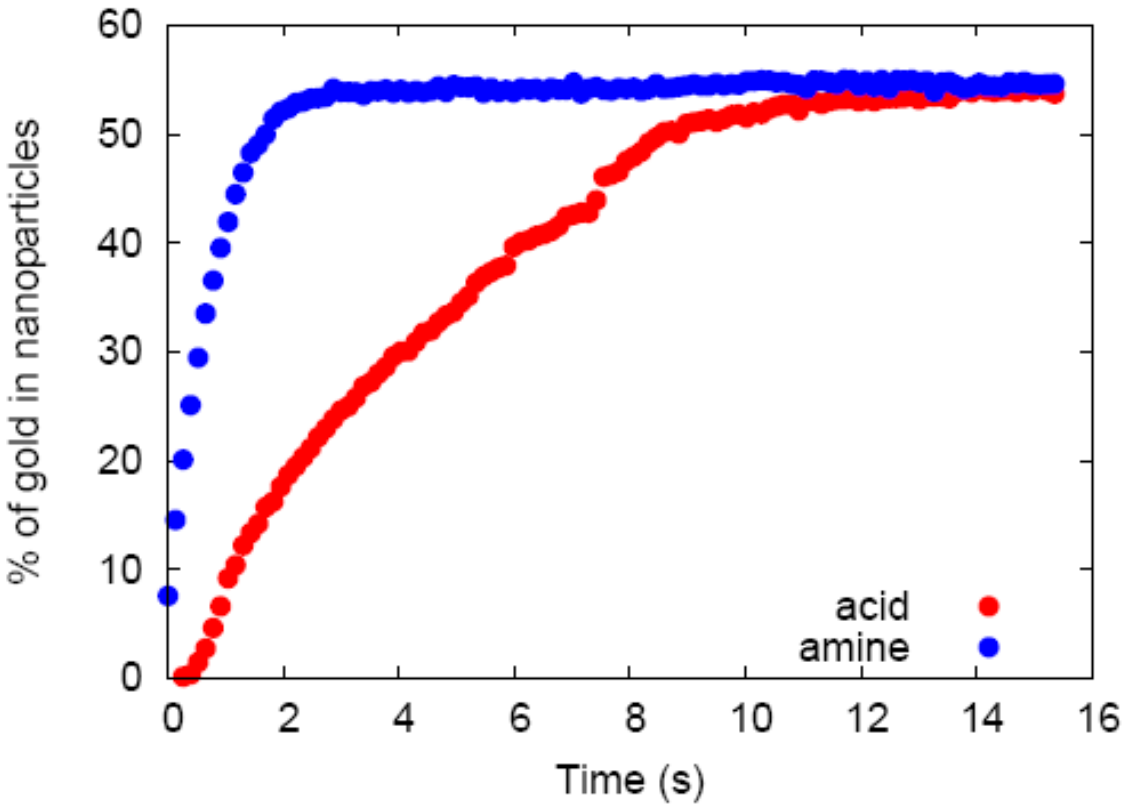

Figure 2: Yield of the reaction as a function of time for the two different ligands obtained via a general property of scattering diagrams.

The results are shown on figure 3 a) for the two different ligands. We observe that the final radius strongly depends on the chemical nature of the ligand (3.5 nm for the acid, 1.4 nm for the amine). Moreover, the kinetics are also different in the first instants of the reaction process. In the acid case, two distinct regimes separated in time can be readily observed. During the first second, there is a burst of the total number of particles while the average radius remains around 1 nm. This behaviour can be ascribed to a nucleation period at the end of which, remarkably, a very little amount (10 %) of the available gold atoms has been consumed, as can be noticed in figure 2. Then, after 1.5 s, the number of growing particles remains almost constant while their radius is increasing by consumption of the remaining atoms in solution thus defining the growth period. In the amine case, the reaction is faster and a burst of nucleation with nearly no growth regime is observed. The nucleation rate is simply deduced by dividing the number density of particles at the end of the nucleation period by the time required to generate these stable nuclei. This global value corresponds to an integration over the instantaneous nucleation rate which strongly depends on the initially increasing supersaturation. A larger nucleation rate is found when amine ligands (1.4810^{18} $L^{-1}.s^{-1}$) are used instead of acid ligands (5.9910^{16} $L^{-1}.s^{-1}$). This can be due to a difference in reducing agent activity. For the acid case, the borohydride (a Lewis base) reacts with the carboxylic acid[18] to produce (tri)acyloxyborohydide, a weaker reducing agent limiting the initial rate of nuclei formation.
The kinetics of growth (only observed with the acid) can either be limited by the diffusion of the monomers towards the surface or by the surface reaction with the monomers.[19] In the two limiting case where one process fully limits the growth, the rate of growth of a particle of radius r is given by a generic differential equation:

$$\frac{dr}{dt} = v_m A \left(C_0 - n^* \frac{4\pi}{3v_m} r^3 - C_{eq}(\infty) e^{r_{cr}/r} \right). \tag{3}$$

where $A = K$ in $\mathrm{nm.s^{-1}}$ for a surface reaction limited growth and $A = \frac{D}{r}$ (D in $\mathrm{nm^2 s^{-1}}$ being the diffusion coefficient of the monomer) for a diffusion limited growth, $C_{eq}(\infty)$ the equilibrium solubility of gold with a macroscopic surface,

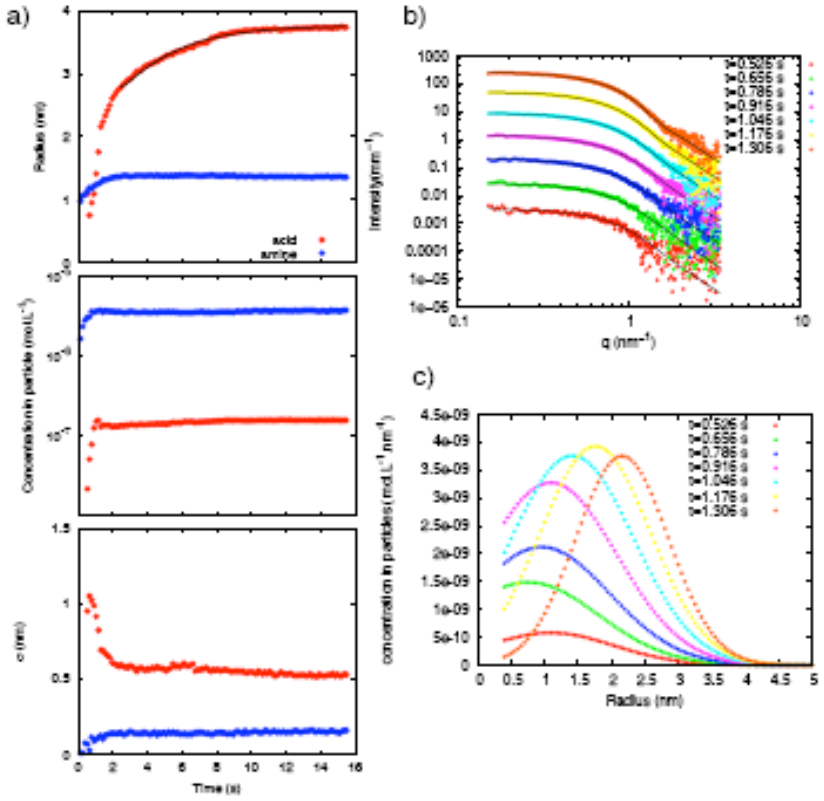

Figure 3: Radius, concentration and size distribution from SAXS fitting a) Results of the fits of the SAXS patterns as a function of time. The concentration in particles ($n * N_A$), the center of the gaussian distribution and the σ parameter are indicated for the two different ligands. b) SAXS patterns for the first instants of the reaction and the corresponding fits for the case of an acid ligand. c) Size distribution corresponding to the SAXS patterns in b).

n^* the number of particles in the solution at the end of the nucleation period and r_{ce} the capillary radius which is linked to the interfacial solid-solvent interfacial tension γ by: $r_{ce} = \frac{2\gamma V_m}{kT}$. The width of the size distribution being small during the whole time of reaction (figure 3 c), the equation 3 is integrated versus time considering a unique type of particles of size r_0. A good fit is obtained for A = $2.0.10^4$ nm.s^{-1} and r_{ce} = 1.2 nm. A typical particle radius of $r = 2$ nm yields a diffusion coefficient (D = 4.0 10^4 nm^2.s^{-1}) four orders of magnitude less than a typical diffusion coefficient of any gold complex species in solution. Thus the growth is limited by the surface reaction with a rate constant of $K = 2(\pm 0.5)10^4$nm.s^{-1}.
Finally, the crystalline nature of the AuNP in formation is given by the *in situ* WAXS results. The appearence and growth of two typical diffraction peaks which belong to FCC gold crystal are clearly observed, one at 31.4 nm^{-1} for the (111) plane and the other at 35.5 nm^{-1} for the (200) plane. The full width at half-maximum of the (111) diffraction peak is constant with time and cannot be linked to the size of the particle. On the contrary, the maximum of the (111) peak increases with time with a charateristic behaviour. The normalised value (relative to the maximum final value) is superimposed to the normalised radius obtained from SAXS (see supporting information). This indicates that the crystallinity of the particles is not modified during the time of the experiment.

The quantitative determination of the number density and size distribution, which in the present case revealed that the ligands impose the AuNp final size by controlling their nucleation rate, opens an effective experimental route towards a comprehensive treatment of the nucleation and growth of nanoparticles.

References

[1] Joo, J.; Yu, T.; Kim, Y. W.; Park, H. M.; Wu, F. X.; Zhang, J. Z.; Hyeon, T. *J. Am. Chem. Soc.* **2003**, *125*, 6553–6557.

[2] Park, J.; An, K. J.; Hwang, Y. S.; Park, J. G.; Noh, H. J.; Kim, J. Y.; Park, J. H.; Hwang, N. M.; Hyeon, T. *Nature Mat.* **2004**, *3*, 891–895.

[3] Manna, L.; Milliron, D. J.; Meisel, A.; Scher, E. C.; Alivisatos, A. P. *Nature Mat.* **2003**, *2*, 382–385.

[4] Yin, Y.; Alivisatos, P. *Nature* **2005**, *437*, 664–670.

[5] Qu, L. H.; Yu, W. W.; Peng, X. P. *Nano Lett.* **2004**, *4*, 465–469.

[6] Bullen, C. R.; Mulvaney, P. *Nano Lett.* **2004**, *4*, 2303–2307.

[7] Daniel, M.; Astruc, D. *Chem. Rev.* **2004**, *104*, 293–346.

[8] Storhoff, J. J.; Elghanian, R.; Mucic, R. C.; Mirkin, C. A.; Letsinger, R. L. *J. Am. Chem. Soc.* **1998**, *120*, 1959–1964.

[9] Bond, G. C.; Thompson, D. T. *Catalysis reviews-science and engineering* **1999**, *41*, 319–388.

[10] Jana, N.; Peng, X. *J. Am. Chem. Soc.* **2003**, *125*, 14280-14281.

[11] Ne, F.; Testard, F.; Zemb, T.; Grillo, I. *Langmuir* **2003**, *19*, 8503–8510.

[12] Weiss, T. M.; Narayanan, T.; Wolf, C.; Gradzielski, M.; Panine, P.; Finet, S.; Helsby, W. I. *Phys. Rev. Lett.* **2005**, *94*, 038303.

[13] Panine, P.; Finet, S.; Weiss, T. M.; Narayanan, T. *Adv. in Coll. and Int. Science* **2006**, *127*, 9–18.

[14] Andreescu, D.; Sau, T. K.; Goia, D. V. *J. Colloid Interface Sci.* **2006**, *298*, 742–751.

[15] Kimling, J.; Maier, M.; Okenve, B.; Kotaidis, V.; Ballot, H.; Plech, A. *J. Phys. Chem. B.* **2006**, *110*, 15700–15707.

[16] Guinier, A.; Fournet, G. *Small Angle Scattering of X-Rays;* Wiley, New York: 1955.

[17] Glatter, O. Small Angle X-ray Scattering. In ; Glatter, O.; Kratky, O., Eds.; Academic Press, London: 1982.

[18] Gribble, G. W. *Chem. Soc. Rev.* **1998**, *27*, 395–404.

[19] Talapin, D. V.; Rogach, A. L.; Haase, M.; Weller, H. *J. Phys. Chem. B.* **2001**, *105*, 12278–12285.